

Search for $\eta_c(2S) \rightarrow \pi^+ \pi^- \eta_c$ and $\eta_c(2S) \rightarrow \pi^+ \pi^- K_S^0 K^\pm \pi^\mp$ decays

M. Ablikim¹, M. N. Achasov^{4,c}, P. Adlarson⁷⁵, O. Afedulidis³, X. C. Ai⁸⁰, R. Aliberti³⁵, A. Amoroso^{74A,74C}, Q. An^{71,58,a}, Y. Bai⁵⁷, O. Bakina³⁶, I. Balossino^{29A}, Y. Ban^{46,h}, H.-R. Bao⁶³, V. Batozskaya^{1,44}, K. Begzsuren³², N. Berger³⁵, M. Berlowski⁴⁴, M. Bertani^{28A}, D. Bettoni^{29A}, F. Bianchi^{74A,74C}, E. Bianco^{74A,74C}, A. Bortone^{74A,74C}, I. Boyko³⁶, R. A. Briere⁵, A. Brueggemann⁶⁸, H. Cai⁷⁶, X. Cai^{1,58}, A. Calcaterra^{28A}, G. F. Cao^{1,63}, N. Cao^{1,63}, S. A. Cetin^{62A}, J. F. Chang^{1,58}, G. R. Che⁴³, G. Chelkov^{36,b}, C. Chen⁴³, C. H. Chen⁹, Chao Chen⁵⁵, G. Chen¹, H. S. Chen^{1,63}, H. Y. Chen²⁰, M. L. Chen^{1,58,63}, S. J. Chen⁴², S. L. Chen⁴⁵, S. M. Chen⁶¹, T. Chen^{1,63}, X. R. Chen^{31,63}, X. T. Chen^{1,63}, Y. B. Chen^{1,58}, Y. Q. Chen³⁴, Z. J. Chen^{25,i}, Z. Y. Chen^{1,63}, S. K. Choi^{10A}, G. Cibinetto^{29A}, F. Cossio^{74C}, J. J. Cui⁵⁰, H. L. Dai^{1,58}, J. P. Dai⁷⁸, A. Dbeysi¹⁸, R. E. de Boer³, D. Dedovich³⁶, C. Q. Deng⁷², Z. Y. Deng¹, A. Denig³⁵, I. Denysenko³⁶, M. Destefanis^{74A,74C}, F. De Mori^{74A,74C}, B. Ding^{66,1}, X. X. Ding^{46,h}, Y. Ding³⁴, Y. Ding⁴⁰, J. Dong^{1,58}, L. Y. Dong^{1,63}, M. Y. Dong^{1,58,63}, X. Dong⁷⁶, M. C. Du¹, S. X. Du⁸⁰, Y. Y. Duan⁵⁵, Z. H. Duan⁴², P. Egorov^{36,b}, Y. H. Fan⁴⁵, J. Fang⁵⁹, J. Fang^{1,58}, S. S. Fang^{1,63}, W. X. Fang¹, Y. Fang¹, Y. Q. Fang^{1,58}, R. Farinelli^{29A}, L. Fava^{74B,74C}, F. Feldbauer³, G. Felici^{28A}, C. Q. Feng^{71,58}, J. H. Feng⁵⁹, Y. T. Feng^{71,58}, M. Fritsch³, C. D. Fu¹, J. L. Fu⁶³, Y. W. Fu^{1,63}, H. Gao⁶³, X. B. Gao⁴¹, Y. N. Gao^{46,h}, Yang Gao^{71,58}, S. Garbolino^{74C}, I. Garzia^{29A,29B}, L. Ge⁸⁰, P. T. Ge⁷⁶, Z. W. Ge⁴², C. Geng⁵⁹, E. M. Gersabeck⁶⁷, A. Gilman⁶⁹, K. Goetzen¹³, L. Gong⁴⁰, W. X. Gong^{1,58}, W. Gradl³⁵, S. Gramigna^{29A,29B}, M. Greco^{74A,74C}, M. H. Gu^{1,58}, Y. T. Gu¹⁵, C. Y. Guan^{1,63}, Z. L. Guan²², A. Q. Guo^{31,63}, L. B. Guo⁴¹, M. J. Guo⁵⁰, R. P. Guo⁴⁹, Y. P. Guo^{12,g}, A. Guskov^{36,b}, J. Gutierrez²⁷, K. L. Han⁶³, T. T. Han¹, F. Hanisch³, X. Q. Hao¹⁹, F. A. Harris⁶⁵, K. K. He⁵⁵, K. L. He^{1,63}, F. H. Heinsius³, C. H. Heinzel³⁵, Y. K. Heng^{1,58,63}, C. Herold⁶⁰, T. Holtmann³, P. C. Hong³⁴, G. Y. Hou^{1,63}, X. T. Hou^{1,63}, Y. R. Hou⁶³, Z. L. Hou¹, B. Y. Hu⁵⁹, H. M. Hu^{1,63}, J. F. Hu^{56,j}, S. L. Hu^{12,g}, T. Hu^{1,58,63}, Y. Hu¹, G. S. Huang^{71,58}, K. X. Huang⁵⁹, L. Q. Huang^{31,63}, X. T. Huang⁵⁰, Y. P. Huang¹, T. Hussain⁷³, F. Hölkken³, N. Hüskens^{27,35}, N. Hüskens³⁵, N. in der Wiesche⁶⁸, J. Jackson²⁷, S. Janchiv³², J. H. Jeong^{10A}, Q. Ji¹, Q. P. Ji¹⁹, W. Ji^{1,63}, X. B. Ji^{1,63}, X. L. Ji^{1,58}, Y. Y. Ji⁵⁰, X. Q. Jia⁵⁰, Z. K. Jia^{71,58}, D. Jiang^{1,63}, H. B. Jiang⁷⁶, P. C. Jiang^{46,h}, S. S. Jiang³⁹, T. J. Jiang¹⁶, X. S. Jiang^{1,58,63}, Y. Jiang⁶³, J. B. Jiao⁵⁰, J. K. Jiao³⁴, Z. Jiao²³, S. Jin⁴², Y. Jin⁶⁶, M. Q. Jing^{1,63}, X. M. Jing⁶³, T. Johansson⁷⁵, S. Kabana³³, N. Kalantar-Nayestanaki⁶⁴, X. L. Kang⁹, X. S. Kang⁴⁰, M. Kavatsyuk⁶⁴, B. C. Ke⁸⁰, V. Khachatryan²⁷, A. Khoukaz⁶⁸, R. Kiuchi¹, O. B. Kolcu^{62A}, B. Kopf³, M. Kuessner³, X. Kui^{1,63}, N. Kumar²⁶, A. Kupsc^{44,75}, W. Kühn³⁷, J. J. Lane⁶⁷, P. Larin¹⁸, L. Lavezzi^{74A,74C}, T. T. Lei^{71,58}, Z. H. Lei^{71,58}, M. Lellmann³⁵, T. Lenz³⁵, C. Li⁴⁷, C. Li⁴³, C. H. Li³⁹, Cheng Li^{71,58}, D. M. Li⁸⁰, F. Li^{1,58}, G. Li¹, H. B. Li^{1,63}, H. J. Li¹⁹, H. N. Li^{56,j}, Hui Li⁴³, J. R. Li⁶¹, J. S. Li⁵⁹, Ke Li¹, L. J. Li^{1,63}, L. K. Li¹, Lei Li⁴⁸, M. H. Li⁴³, P. R. Li^{38,l}, Q. M. Li^{1,63}, Q. X. Li⁵⁰, R. Li^{17,31}, S. X. Li¹², T. Li⁵⁰, W. D. Li^{1,63}, W. G. Li^{1,a}, X. Li^{1,63}, X. H. Li^{71,58}, X. L. Li⁵⁰, X. Z. Li⁵⁹, Xiaoyu Li^{1,63}, Y. G. Li^{46,h}, Z. J. Li⁵⁹, Z. X. Li¹⁵, Z. Y. Li⁷⁸, C. Liang⁴², H. Liang^{71,58}, H. Liang^{1,63}, Y. F. Liang⁵⁴, Y. T. Liang^{31,63}, G. R. Liao¹⁴, L. Z. Liao⁵⁰, J. Libby²⁶, A. Limphirat⁶⁰, C. C. Lin⁵⁵, D. X. Lin^{31,63}, T. Lin¹, B. J. Liu¹, B. X. Liu⁷⁶, C. Liu³⁴, C. X. Liu¹, F. H. Liu⁵³, Fang Liu¹, Feng Liu⁶, G. M. Liu^{56,j}, H. Liu^{38,k,l}, H. B. Liu¹⁵, H. M. Liu^{1,63}, Huanhuan Liu¹, Huihui Liu²¹, J. B. Liu^{71,58}, J. Y. Liu^{1,63}, K. Liu^{38,k,l}, K. Y. Liu⁴⁰, Ke Liu²², L. Liu^{71,58}, L. C. Liu⁴³, Lu Liu⁴³, M. H. Liu^{12,g}, P. L. Liu¹, Q. Liu⁶³, S. B. Liu^{71,58}, T. Liu^{12,g}, W. K. Liu⁴³, W. M. Liu^{71,58}, X. Liu³⁹, X. Liu^{38,k,l}, Y. Liu^{38,k,l}, Y. Liu⁸⁰, Y. B. Liu⁴³, Z. A. Liu^{1,58,63}, Z. D. Liu⁹, Z. Q. Liu⁵⁰, X. C. Lou^{1,58,63}, F. X. Lu⁵⁹, H. J. Lu²³, J. G. Lu^{1,58}, X. L. Lu¹, Y. Lu⁷, Y. P. Lu^{1,58}, Z. H. Lu^{1,63}, C. L. Luo⁴¹, M. X. Luo⁷⁹, T. Luo^{12,g}, X. L. Luo^{1,58}, X. R. Lyu⁶³, Y. F. Lyu⁴³, F. C. Ma⁴⁰, H. Ma⁷⁸, H. L. Ma¹, J. L. Ma^{1,63}, L. L. Ma⁵⁰, M. M. Ma^{1,63}, Q. M. Ma¹, R. Q. Ma^{1,63}, T. Ma^{71,58}, X. T. Ma^{1,63}, X. Y. Ma^{1,58}, Y. Ma^{46,h}, Y. M. Ma³¹, F. E. Maas¹⁸, M. Maggiora^{74A,74C}, S. Malde⁶⁰, Y. J. Mao^{46,h}, Z. P. Mao¹, S. Marcello^{74A,74C}, Z. X. Meng⁶⁶, J. G. Messchendorp^{13,64}, G. Mezzadri^{29A}, H. Miao^{1,63}, T. J. Min⁴², R. E. Mitchell²⁷, X. H. Mo^{1,58,63}, B. Moses²⁷, N. Yu. Muchnoi^{4,c}, J. Muskalla³⁵, Y. Nefedov³⁶, F. Nerling^{18,e}, L. S. Nie²⁰, I. B. Nikolaev^{4,c}, Z. Ning^{1,58}, S. Nisar^{11,m}, Q. L. Niu^{38,k,l}, W. D. Niu⁵⁵, Y. Niu⁵⁰, S. L. Olsen⁶³, Q. Ouyang^{1,58,63}, S. Pacetti^{28B,28C}, X. Pan⁵⁵, Y. Pan⁵⁷, A. Pathak³⁴, P. Patteri^{28A}, Y. P. Pei^{71,58}, M. Pelizaeus³, H. P. Peng^{71,58}, Y. Y. Peng^{38,k,l}, K. Peters^{13,e}, J. L. Ping⁴¹, R. G. Ping^{1,63}, S. Plura³⁵, V. Prasad³³, F. Z. Qi¹, H. Qi^{71,58}, H. R. Qi⁶¹, M. Qi⁴², T. Y. Qi^{12,g}, S. Qian^{1,58}, W. B. Qian⁶³, C. F. Qiao⁶³, X. K. Qiao⁸⁰, J. J. Qin⁷², L. Q. Qin¹⁴, L. Y. Qin^{71,58}, X. S. Qin⁵⁰, Z. H. Qin^{1,58}, J. F. Qiu¹, Z. H. Qu⁷², C. F. Redmer³⁵, K. J. Ren³⁹, A. Rivetti^{74C}, M. Rolo^{74C}, G. Rong^{1,63}, Ch. Rosner¹⁸, S. N. Ruan⁴³, N. Salone⁴⁴, A. Sarantsev^{36,d}, Y. Schelhaas³⁵, K. Schoenning⁷⁵, M. Scodeggio^{29A}, K. Y. Shan^{12,g}, W. Shan²⁴, X. Y. Shan^{71,58}, Z. J. Shang^{38,k,l}, J. F. Shangguan⁵⁵, L. G. Shao^{1,63}, M. Shao^{71,58}, C. P. Shen^{12,g}, H. F. Shen^{1,8}, W. H. Shen⁶³, X. Y. Shen^{1,63}, B. A. Shi⁶³, H. Shi^{71,58}, H. C. Shi^{71,58}, J. L. Shi^{12,g}, J. Y. Shi¹, Q. Q. Shi⁵⁵, S. Y. Shi⁷², X. Shi^{1,58}, J. J. Song¹⁹, T. Z. Song⁵⁹, W. M. Song^{34,1}, Y. J. Song^{12,g}, Y. X. Song^{46,h,n}, S. Sosio^{74A,74C}, S. Spataro^{74A,74C}, F. Stieler³⁵, Y. J. Su⁶³,

G. B. Sun⁷⁶, G. X. Sun¹, H. Sun⁶³, H. K. Sun¹, J. F. Sun¹⁹, K. Sun⁶¹, L. Sun⁷⁶, S. S. Sun^{1,63}, T. Sun^{51,f}, W. Y. Sun³⁴, Y. Sun⁹, Y. J. Sun^{71,58}, Y. Z. Sun¹, Z. Q. Sun^{1,63}, Z. T. Sun⁵⁰, C. J. Tang⁵⁴, G. Y. Tang¹, J. Tang⁵⁹, M. Tang^{71,58}, Y. A. Tang⁷⁶, L. Y. Tao⁷², Q. T. Tao^{25,i}, M. Tat⁶⁹, J. X. Teng^{71,58}, V. Thoren⁷⁵, W. H. Tian⁵⁹, Y. Tian^{31,63}, Z. F. Tian⁷⁶, I. Uman^{62B}, Y. Wan⁵⁵, S. J. Wang⁵⁰, B. Wang¹, B. L. Wang⁶³, Bo Wang^{71,58}, D. Y. Wang^{46,h}, F. Wang⁷², H. J. Wang^{38,k,l}, J. J. Wang⁷⁶, J. P. Wang⁵⁰, K. Wang^{1,58}, L. L. Wang¹, M. Wang⁵⁰, Meng Wang^{1,63}, N. Y. Wang⁶³, S. Wang^{38,k,l}, S. Wang^{12,g}, T. Wang^{12,g}, T. J. Wang⁴³, W. Wang⁷², W. Wang⁵⁹, W. P. Wang^{35,71,o}, X. Wang^{46,h}, X. F. Wang^{38,k,l}, X. J. Wang³⁹, X. L. Wang^{12,g}, X. N. Wang¹, Y. Wang⁶¹, Y. D. Wang⁴⁵, Y. F. Wang^{1,58,63}, Y. L. Wang¹⁹, Y. N. Wang⁴⁵, Y. Q. Wang¹, Yaqian Wang¹⁷, Yi Wang⁶¹, Z. Wang^{1,58}, Z. L. Wang⁷², Z. Y. Wang^{1,63}, Ziyi Wang⁶³, D. H. Wei¹⁴, F. Weidner⁶⁸, S. P. Wen¹, Y. R. Wen³⁹, U. Wiedner³, G. Wilkinson⁶⁹, M. Wolke⁷⁵, L. Wollenberg³, C. Wu³⁹, J. F. Wu^{1,8}, L. H. Wu¹, L. J. Wu^{1,63}, X. Wu^{12,g}, X. H. Wu³⁴, Y. Wu^{71,58}, Y. H. Wu⁵⁵, Y. J. Wu³¹, Z. Wu^{1,58}, L. Xia^{71,58}, X. M. Xian³⁹, B. H. Xiang^{1,63}, T. Xiang^{46,h}, D. Xiao^{38,k,l}, G. Y. Xiao⁴², S. Y. Xiao¹, Y. L. Xiao^{12,g}, Z. J. Xiao⁴¹, C. Xie⁴², X. H. Xie^{46,h}, Y. Xie⁵⁰, Y. G. Xie^{1,58}, Y. H. Xie⁶, Z. P. Xie^{71,58}, T. Y. Xing^{1,63}, C. F. Xu^{1,63}, C. J. Xu⁵⁹, G. F. Xu¹, H. Y. Xu⁶⁶, M. Xu^{71,58}, Q. J. Xu¹⁶, Q. N. Xu³⁰, W. Xu¹, W. L. Xu⁶⁶, X. P. Xu⁵⁵, Y. C. Xu⁷⁷, Z. P. Xu⁴², Z. S. Xu⁶³, F. Yan^{12,g}, L. Yan^{12,g}, W. B. Yan^{71,58}, W. C. Yan⁸⁰, X. Q. Yan¹, H. J. Yang^{51,f}, H. L. Yang³⁴, H. X. Yang¹, Tao Yang¹, Y. Yang^{12,g}, Y. F. Yang⁴³, Y. X. Yang^{1,63}, Yifan Yang^{1,63}, Z. W. Yang^{38,k,l}, Z. P. Yao⁵⁰, M. Ye^{1,58}, M. H. Ye⁸, J. H. Yin¹, Z. Y. You⁵⁹, B. X. Yu^{1,58,63}, C. X. Yu⁴³, G. Yu^{1,63}, J. S. Yu^{25,i}, T. Yu⁷², X. D. Yu^{46,h}, Y. C. Yu⁸⁰, C. Z. Yuan^{1,63}, J. Yuan³⁴, L. Yuan², S. C. Yuan¹, Y. Yuan^{1,63}, Y. J. Yuan⁴⁵, Z. Y. Yuan⁵⁹, C. X. Yue³⁹, A. A. Zafar⁷³, F. R. Zeng⁵⁰, S. H. Zeng⁷², X. Zeng^{12,g}, Y. Zeng^{25,i}, Y. J. Zeng⁵⁹, X. Y. Zhai³⁴, Y. C. Zhai⁵⁰, Y. H. Zhan⁵⁹, A. Q. Zhang^{1,63}, B. L. Zhang^{1,63}, B. X. Zhang¹, D. H. Zhang⁴³, G. Y. Zhang¹⁹, H. Zhang⁸⁰, H. Zhang^{71,58}, H. C. Zhang^{1,58,63}, H. H. Zhang⁵⁹, H. H. Zhang³⁴, H. Q. Zhang^{1,58,63}, H. R. Zhang^{71,58}, H. Y. Zhang^{1,58}, J. Zhang⁸⁰, J. Zhang⁵⁹, J. J. Zhang⁵², J. L. Zhang²⁰, J. Q. Zhang⁴¹, J. S. Zhang^{12,g}, J. W. Zhang^{1,58,63}, J. X. Zhang^{38,k,l}, J. Y. Zhang¹, J. Z. Zhang^{1,63}, Jianyu Zhang⁶³, L. M. Zhang⁶¹, Lei Zhang⁴², P. Zhang^{1,63}, Q. Y. Zhang³⁴, R. Y. Zhang^{38,k,l}, Shuihan Zhang^{1,63}, Shulei Zhang^{25,i}, X. D. Zhang⁴⁵, X. M. Zhang¹, X. Y. Zhang⁵⁰, Y. Zhang⁷², Y. T. Zhang⁸⁰, Y. H. Zhang^{1,58}, Y. M. Zhang³⁹, Yan Zhang^{71,58}, Yao Zhang¹, Z. D. Zhang¹, Z. H. Zhang¹, Z. L. Zhang³⁴, Z. Y. Zhang⁷⁶, Z. Y. Zhang⁴³, Z. Z. Zhang⁴⁵, G. Zhao¹, J. Y. Zhao^{1,63}, J. Z. Zhao^{1,58}, Lei Zhao^{71,58}, Ling Zhao¹, M. G. Zhao⁴³, N. Zhao⁷⁸, R. P. Zhao⁶³, S. J. Zhao⁸⁰, Y. B. Zhao^{1,58}, Y. X. Zhao^{31,63}, Z. G. Zhao^{71,58}, A. Zhemchugov^{36,b}, B. Zheng⁷², B. M. Zheng³⁴, J. P. Zheng^{1,58}, W. J. Zheng^{1,63}, Y. H. Zheng⁶³, B. Zhong⁴¹, X. Zhong⁵⁹, H. Zhou⁵⁰, J. Y. Zhou³⁴, L. P. Zhou^{1,63}, S. Zhou⁶, X. Zhou⁷⁶, X. K. Zhou⁶, X. R. Zhou^{71,58}, X. Y. Zhou³⁹, Y. Z. Zhou^{12,g}, J. Zhu⁴³, K. Zhu¹, K. J. Zhu^{1,58,63}, K. S. Zhu^{12,g}, L. Zhu³⁴, L. X. Zhu⁶³, S. H. Zhu⁷⁰, S. Q. Zhu⁴², T. J. Zhu^{12,g}, W. D. Zhu⁴¹, Y. C. Zhu^{71,58}, Z. A. Zhu^{1,63}, J. H. Zou¹, J. Zu^{71,58}

(BESIII Collaboration)

¹ Institute of High Energy Physics, Beijing 100049, People's Republic of China

² Beihang University, Beijing 100191, People's Republic of China

³ Bochum Ruhr-University, D-44780 Bochum, Germany

⁴ Budker Institute of Nuclear Physics SB RAS (BINP), Novosibirsk 630090, Russia

⁵ Carnegie Mellon University, Pittsburgh, Pennsylvania 15213, USA

⁶ Central China Normal University, Wuhan 430079, People's Republic of China

⁷ Central South University, Changsha 410083, People's Republic of China

⁸ China Center of Advanced Science and Technology, Beijing 100190, People's Republic of China

⁹ China University of Geosciences, Wuhan 430074, People's Republic of China

¹⁰ Chung-Ang University, Seoul, 06974, Republic of Korea

¹¹ COMSATS University Islamabad, Lahore Campus, Defence Road, Off Raiwind Road, 54000 Lahore, Pakistan

¹² Fudan University, Shanghai 200433, People's Republic of China

¹³ GSI Helmholtzcentre for Heavy Ion Research GmbH, D-64291 Darmstadt, Germany

¹⁴ Guangxi Normal University, Guilin 541004, People's Republic of China

¹⁵ Guangxi University, Nanning 530004, People's Republic of China

¹⁶ Hangzhou Normal University, Hangzhou 310036, People's Republic of China

¹⁷ Hebei University, Baoding 071002, People's Republic of China

¹⁸ Helmholtz Institute Mainz, Staudinger Weg 18, D-55099 Mainz, Germany

¹⁹ Henan Normal University, Xinxiang 453007, People's Republic of China

²⁰ Henan University, Kaifeng 475004, People's Republic of China

²¹ Henan University of Science and Technology, Luoyang 471003, People's Republic of China

- ²² Henan University of Technology, Zhengzhou 450001, People's Republic of China
²³ Huangshan College, Huangshan 245000, People's Republic of China
²⁴ Hunan Normal University, Changsha 410081, People's Republic of China
²⁵ Hunan University, Changsha 410082, People's Republic of China
²⁶ Indian Institute of Technology Madras, Chennai 600036, India
²⁷ Indiana University, Bloomington, Indiana 47405, USA
- ²⁸ INFN Laboratori Nazionali di Frascati , (A)INFN Laboratori Nazionali di Frascati, I-00044, Frascati, Italy; (B)INFN Sezione di Perugia, I-06100, Perugia, Italy; (C)University of Perugia, I-06100, Perugia, Italy
²⁹ INFN Sezione di Ferrara, (A)INFN Sezione di Ferrara, I-44122, Ferrara, Italy; (B)University of Ferrara, I-44122, Ferrara, Italy
- ³⁰ Inner Mongolia University, Hohhot 010021, People's Republic of China
³¹ Institute of Modern Physics, Lanzhou 730000, People's Republic of China
³² Institute of Physics and Technology, Peace Avenue 54B, Ulaanbaatar 13330, Mongolia
³³ Instituto de Alta Investigación, Universidad de Tarapacá, Casilla 7D, Arica 1000000, Chile
³⁴ Jilin University, Changchun 130012, People's Republic of China
- ³⁵ Johannes Gutenberg University of Mainz, Johann-Joachim-Becher-Weg 45, D-55099 Mainz, Germany
³⁶ Joint Institute for Nuclear Research, 141980 Dubna, Moscow region, Russia
- ³⁷ Justus-Liebig-Universitaet Giessen, II. Physikalisches Institut, Heinrich-Buff-Ring 16, D-35392 Giessen, Germany
³⁸ Lanzhou University, Lanzhou 730000, People's Republic of China
- ³⁹ Liaoning Normal University, Dalian 116029, People's Republic of China
⁴⁰ Liaoning University, Shenyang 110036, People's Republic of China
⁴¹ Nanjing Normal University, Nanjing 210023, People's Republic of China
⁴² Nanjing University, Nanjing 210093, People's Republic of China
⁴³ Nankai University, Tianjin 300071, People's Republic of China
⁴⁴ National Centre for Nuclear Research, Warsaw 02-093, Poland
- ⁴⁵ North China Electric Power University, Beijing 102206, People's Republic of China
⁴⁶ Peking University, Beijing 100871, People's Republic of China
⁴⁷ Qufu Normal University, Qufu 273165, People's Republic of China
⁴⁸ Renmin University of China, Beijing 100872, People's Republic of China
⁴⁹ Shandong Normal University, Jinan 250014, People's Republic of China
⁵⁰ Shandong University, Jinan 250100, People's Republic of China
- ⁵¹ Shanghai Jiao Tong University, Shanghai 200240, People's Republic of China
⁵² Shanxi Normal University, Linfen 041004, People's Republic of China
⁵³ Shanxi University, Taiyuan 030006, People's Republic of China
⁵⁴ Sichuan University, Chengdu 610064, People's Republic of China
⁵⁵ Soochow University, Suzhou 215006, People's Republic of China
- ⁵⁶ South China Normal University, Guangzhou 510006, People's Republic of China
⁵⁷ Southeast University, Nanjing 211100, People's Republic of China
⁵⁸ State Key Laboratory of Particle Detection and Electronics, Beijing 100049, Hefei 230026, People's Republic of China
⁵⁹ Sun Yat-Sen University, Guangzhou 510275, People's Republic of China
- ⁶⁰ Suranaree University of Technology, University Avenue 111, Nakhon Ratchasima 30000, Thailand
⁶¹ Tsinghua University, Beijing 100084, People's Republic of China
- ⁶² Turkish Accelerator Center Particle Factory Group, (A)Istinye University, 34010, Istanbul, Turkey; (B)Near East University, Nicosia, North Cyprus, 99138, Mersin 10, Turkey
- ⁶³ University of Chinese Academy of Sciences, Beijing 100049, People's Republic of China
⁶⁴ University of Groningen, NL-9747 AA Groningen, The Netherlands
⁶⁵ University of Hawaii, Honolulu, Hawaii 96822, USA
⁶⁶ University of Jinan, Jinan 250022, People's Republic of China
- ⁶⁷ University of Manchester, Oxford Road, Manchester, M13 9PL, United Kingdom
⁶⁸ University of Muenster, Wilhelm-Klemm-Strasse 9, 48149 Muenster, Germany
⁶⁹ University of Oxford, Keble Road, Oxford OX13RH, United Kingdom
- ⁷⁰ University of Science and Technology Liaoning, Anshan 114051, People's Republic of China

⁷¹ University of Science and Technology of China, Hefei 230026, People's Republic of China

⁷² University of South China, Hengyang 421001, People's Republic of China

⁷³ University of the Punjab, Lahore-54590, Pakistan

⁷⁴ University of Turin and INFN, (A)University of Turin, I-10125, Turin, Italy; (B)University of Eastern Piedmont, I-15121, Alessandria, Italy; (C)INFN, I-10125, Turin, Italy

⁷⁵ Uppsala University, Box 516, SE-75120 Uppsala, Sweden

⁷⁶ Wuhan University, Wuhan 430072, People's Republic of China

⁷⁷ Yantai University, Yantai 264005, People's Republic of China

⁷⁸ Yunnan University, Kunming 650500, People's Republic of China

⁷⁹ Zhejiang University, Hangzhou 310027, People's Republic of China

⁸⁰ Zhengzhou University, Zhengzhou 450001, People's Republic of China

^a Deceased

^b Also at the Moscow Institute of Physics and Technology, Moscow 141700, Russia

^c Also at the Novosibirsk State University, Novosibirsk, 630090, Russia

^d Also at the NRC "Kurchatov Institute", PNPI, 188300, Gatchina, Russia

^e Also at Goethe University Frankfurt, 60323 Frankfurt am Main, Germany

^f Also at Key Laboratory for Particle Physics, Astrophysics and Cosmology, Ministry of Education; Shanghai Key Laboratory for Particle Physics and Cosmology; Institute of Nuclear and Particle Physics, Shanghai 200240, People's Republic of China

^g Also at Key Laboratory of Nuclear Physics and Ion-beam Application (MOE) and Institute of Modern Physics, Fudan University, Shanghai 200443, People's Republic of China

^h Also at State Key Laboratory of Nuclear Physics and Technology, Peking University, Beijing 100871, People's Republic of China

ⁱ Also at School of Physics and Electronics, Hunan University, Changsha 410082, China

^j Also at Guangdong Provincial Key Laboratory of Nuclear Science, Institute of Quantum Matter, South China Normal University, Guangzhou 510006, China

^k Also at MOE Frontiers Science Center for Rare Isotopes, Lanzhou University, Lanzhou 730000, People's Republic of China

^l Also at Lanzhou Center for Theoretical Physics, Lanzhou University, Lanzhou 730000, People's Republic of China

^m Also at the Department of Mathematical Sciences, IBA, Karachi 75270, Pakistan

ⁿ Also at Ecole Polytechnique Federale de Lausanne (EPFL), CH-1015 Lausanne, Switzerland

^o Also at Helmholtz Institute Mainz, Staudinger Weg 18, D-55099 Mainz, Germany

Based on $(27.12 \pm 0.14) \times 10^8$ $\psi(2S)$ events collected with the BESIII detector, we search for the decay $\eta_c(2S) \rightarrow \pi^+ \pi^- \eta_c$ with $\eta_c \rightarrow K_S^0 K^\pm \pi^\mp$ and $\eta_c \rightarrow K^+ K^- \pi^0$. No significant signal is observed, and the upper limit on the product branching fraction $\mathcal{B}(\psi(2S) \rightarrow \gamma \eta_c(2S)) \times \mathcal{B}(\eta_c(2S) \rightarrow \pi^+ \pi^- \eta_c)$ is determined to be 2.21×10^{-5} at the 90% confidence level. In addition, the analysis of the process $\psi(2S) \rightarrow \gamma \eta_c(2S)$, $\eta_c(2S) \rightarrow \pi^+ \pi^- K_S^0 K^\pm \pi^\mp$ gives a clear $\eta_c(2S)$ signal with a statistical significance of 10σ for the first time, and the branching fraction $\mathcal{B}(\eta_c(2S) \rightarrow \pi^+ \pi^- K_S^0 K^\pm \pi^\mp)$ is determined to be $(1.33 \pm 0.11 \pm 0.4 \pm 0.95) \times 10^{-2}$, where the first uncertainty is statistical, the second is systematic, and the third uncertainty is due to the quoted $\mathcal{B}(\psi(2S) \rightarrow \gamma \eta_c(2S))$.

I. INTRODUCTION

Charmonium states play an important role in understanding the strong interaction. Despite being known for more than half a century, the charmonium system still leaves much room for further study, especially in the spin singlet sector [1] which includes the 1P_1 state h_c and the 1S_0 state $\eta_c(2S)$. The $\eta_c(2S)$ is the first excited state of the pseudoscalar ground state η_c , lying just below the mass of its vector counterpart, $\psi(2S)$ [1]. It was first observed by the Belle collaboration [2] in the process $B^\pm \rightarrow K^\pm \eta_c(2S)$ with $\eta_c(2S) \rightarrow K_S^0 K^\pm \pi^\mp$. The $\eta_c(2S)$ was subsequently confirmed by BaBar [3],

CLEO [4], and Belle [5] in $\gamma\gamma$ -fusion to $K\bar{K}\pi$ final state, by BaBar [6] in double charmonium production process $e^+e^- \rightarrow J/\psi c\bar{c}$ and Belle [7] in the inclusive process $e^+e^- \rightarrow J/\psi + \text{anything}$. BESIII studied $\psi(2S) \rightarrow \gamma \eta_c(2S)$ with $\eta_c(2S) \rightarrow K_S^0 K^\pm \pi^\mp$ and $\eta_c(2S) \rightarrow K^+ K^- \pi^0$ [8], and showed consistent results with previous experimental measurements and theoretical calculations.

Exploring hadronic transitions between charmonium states offers a valuable opportunity to study the dynamics of heavy quarks. Experimental [9] and theoretical [10, 11] investigations have provided a comprehensive understanding of those processes involving the emission of

two-pion in the low energy chiral dynamics framework. Such decays are described as that heavy quarkonium transition generates a soft gluonic field which then produces the light mesons in QCD picture. The two-pion transition between 1S_0 states of the charmonium have not yet been observed.

The transition amplitude of the $\eta_c(2S) \rightarrow \pi^+ \pi^- \eta_c$ decay [12] is expected to have the same linear dependence q^2 as the $\psi(2S) \rightarrow \pi^+ \pi^- J/\psi$ decay [13], where q is the total 4-momentum of the pion pair. By estimating only the phase space (PHSP) in the single-channel approach, the branching fraction of $\eta_c(2S) \rightarrow \pi^+ \pi^- \eta_c$ is estimated to be $\sim 5\%$ [12, 14]. This decay may be further suppressed due to the contribution of the chromo-magnetic interaction in the decay amplitude [15].

A previous study indicated that the $\eta_c(2S) \rightarrow \pi^+ \pi^- \eta_c$ decay is the most probable decay mode of $\eta_c(2S)$ [12]. The BaBar collaboration set the 90% confidence level (C.L.) upper limit of $\mathcal{B}(\eta_c(2S) \rightarrow \pi^+ \pi^- \eta_c) < 7.4\%$ based on the $e^+ e^-$ collision data, corresponding to an integrated luminosity of $(429.1 \pm 1.9) \text{ fb}^{-1}$ collected at the $\Upsilon(4S)$ resonance [16]. In recent years, the BESIII collaboration collected a large data sample of $\psi(2S)$, which provides a great opportunity to search for $\eta_c(2S) \rightarrow \pi^+ \pi^- \eta_c$ and validate the theoretical calculations [10, 11].

To date, only a few decay modes of $\eta_c(2S)$ have been observed, therefore, searching for new decay modes is important for an in-depth understanding of its properties. Using 106 million $\psi(2S)$ events collected by the BESIII detector, an evidence for the decay $\eta_c(2S) \rightarrow \pi^+ \pi^- K_S^0 K^\pm \pi^\mp$ is found with a statistical significance of greater than 4σ [17]. With $(27.12 \pm 0.14) \times 10^8$ $\psi(2S)$ events taken by the BESIII detector, which is about 25 times larger than the previous data sample [17], we perform a search for $\eta_c(2S) \rightarrow \pi^+ \pi^- \eta_c$ and an improved measurement of the branching fraction of $\eta_c(2S) \rightarrow \pi^+ \pi^- K_S^0 K^\pm \pi^\mp$.

II. BESIII DETECTOR AND MONTE CARLO SIMULATION

The BESIII detector [18] records symmetric $e^+ e^-$ collisions provided by the BEPCII storage ring [19] in the center-of-mass energy range from 2.0 to 4.95 GeV, with a peak luminosity of $1 \times 10^{33} \text{ cm}^{-2} \text{s}^{-1}$ achieved at $\sqrt{s} = 3.77 \text{ GeV}$. BESIII has collected large data samples in this energy region [20] [21]. The cylindrical core of the BESIII detector consists of a helium-based main drift chamber (MDC), a plastic scintillator time-of-flight (TOF) system, and a CsI(Tl) electromagnetic calorimeter (EMC), which are all enclosed in a super conducting solenoidal magnet providing a 1.0 T magnetic field. The solenoid is supported by an octagonal flux-return yoke with resistive plate counter modules interleaved with steel for muon identification. The acceptance for charged particles and photons is 93% of the full solid angle, and the charged-particle momentum resolution at 1 GeV/c is 0.5%. The

photon energy resolution is 2.5% (5%) at 1.0 GeV in the barrel (end-cap) region. The time resolution in the TOF barrel region is 68 ps, while that in the end-cap region was 110 ps. The end-cap TOF system was upgraded in 2015 using multigap resistive plate chamber technology, providing a time resolution of 60 ps, which benefits $\sim 84\%$ of the data used in this analysis [22–24].

Simulated data samples produced with a GEANT4-based Monte Carlo (MC) package [25], which includes the geometric description of the BESIII detector and the detector response, are used to determine detection efficiencies and to estimate backgrounds. The simulation models the beam-energy spread and initial-state radiation (ISR) in $e^+ e^-$ annihilations with the generator KKMC [26, 27]. An inclusive MC sample of 2.7 billion $\psi(3686)$ events is used to investigate potential background. The inclusive MC sample includes the production of the $\psi(3686)$ resonance, the ISR production of the J/ψ , and the continuum processes incorporated in KKMC. The known particle decays are modelled with EVTGEN [28, 29] using branching fractions taken from the Particle Data Group [14], while the remaining unknown decays are estimated with LUNDCHARM [30, 31].

To estimate the signal selection efficiency, detector resolution and background, several exclusive MC samples are generated. Specific generators are employed for channels $\psi(2S) \rightarrow \gamma \eta_c(2S)$ and $\gamma \chi_{c1,2}$, which are based on specialized models that have been packaged and customized specifically for BESIII detector. The polar angle (θ_γ) of the radiation photon in the rest frame of $\psi(2S)$ follows $(1 + \lambda \cos^2 \theta_\gamma)$ function, where the value of λ is 1 for $\eta_c(2S)$, -1/3 for χ_{c1} and 1/13 for χ_{c2} , respectively [32]. Two decay modes $\eta_c \rightarrow K^+ K^- \pi^0$ and $\eta_c \rightarrow K_S^0 K^\pm \pi^\mp$ are generated according to the Dalitz distribution measured by BESIII [33]. The exclusive MC samples $\psi(2S) \rightarrow \gamma \pi^+ \pi^- K_S^0 K^\pm \pi^\mp$ ($\gamma \pi^+ \pi^- K^+ K^- \pi^0$), $\psi(2S) \rightarrow \pi^0 \pi^+ \pi^- K_S^0 K^\pm \pi^\mp$ ($\pi^0 \pi^+ \pi^- K^+ K^- \pi^0$), $\psi(2S) \rightarrow (\gamma_{\text{FSR}}) \pi^+ \pi^- K_S^0 K^\pm \pi^\mp$ ($(\gamma_{\text{FSR}}) \pi^+ \pi^- K^+ K^- \pi^0$) (here, γ_{FSR} stands for a photon from final state radiation), are generated uniformly in the phase space(PHSP).

The data sample collected at the center-of-mass energies of 3.65 GeV, corresponding to integrated luminosity of 410 pb^{-1} , is used to estimate the non-resonant continuum background contributions.

III. MEASUREMENT OF $\eta_c(2S) \rightarrow \pi^+ \pi^- \eta_c$

A. Event selection

In this analysis, η_c is reconstructed with $K_S^0 K^\pm \pi^\mp$ and $K^+ K^- \pi^0$, where K_S^0 (π^0) is reconstructed with pairs of $\pi^+ \pi^-$ ($\gamma \gamma$).

Charged tracks are reconstructed in the MDC using good helix fits, and are required to satisfy $|\cos\theta| < 0.93$, where θ is the polar angle with respect to the z -axis which is the symmetry axis of the MDC. For charged tracks

apart from the K_S^0 decays, the distance of the closest approach to the interaction point must be less than 10 cm along the z -axis, and less than 1 cm in the transverse plane. By combining the dE/dx and TOF information, the $\chi_{\text{PID}}^2(i)$ ($i = K, \pi$, or p) is calculated for each charged track for each hadron i hypothesis. Both PID and kinematic fit information are used to determine the particle type of each charged track, as discussed below.

Photon candidates are identified using showers in the EMC. The deposited energy of each shower must be greater than 25 MeV in the barrel region ($|\cos\theta| < 0.80$) and in the end-cap region ($0.86 < |\cos\theta| < 0.92$). To reduce electronic noise and showers unrelated to the event, the difference between the EMC time and the event start time is required to be within [0, 700] ns. The angle subtended by the EMC shower and the position of the closest extrapolated charged track at the EMC must be greater than 10 degrees. Candidate events must have at least one good photon (three good photons) for the decay mode $\eta_c \rightarrow K_S^0 K^\pm \pi^\mp$ ($\eta_c \rightarrow K^+ K^- \pi^0$).

π^0 Candidates are selected with the invariant mass of $\gamma\gamma$ pair satisfying $|M_{\gamma\gamma} - m_{\pi^0}| < 0.015 \text{ GeV}/c^2$, where m_{π^0} is the known mass of π^0 [14]. To improve the energy resolution, a one-constraint (1C) kinematic fit is performed with the π^0 mass constraint. A kinematic constraint between the production and decay vertices, and a second vertex fit algorithm based on the least square method are employed for K_S^0 candidate. The K_S^0 candidate must be satisfied with a decay length more than 2 standard deviations of the vertex resolution away from the interaction point, and its invariant mass to be within $0.02 \text{ GeV}/c^2$ of the K_S^0 known mass [14]. The events with $|M_{K_S^0 K^\pm \pi^\mp(K^+ K^- \pi^0)} - m_{\eta_c}| < 0.05 \text{ GeV}/c^2$ are selected for further analysis, where $M_{K_S^0 K^\pm \pi^\mp(K^+ K^- \pi^0)}$ is the invariant mass of $K_S^0 K^\pm \pi^\mp(K^+ K^- \pi^0)$ and m_{η_c} is the known mass of η_c meson [14].

For the process of $\eta_c(2S) \rightarrow \pi^+ \pi^- \eta_c$, $\eta_c \rightarrow K^+ K^- \pi^0$, a five-constraints (5C) kinematic fit is performed with the constraints of total four-momentum conservation and two photons with the invariant mass constrained to the known π^0 mass. For the process of $\eta_c(2S) \rightarrow \pi^+ \pi^- \eta_c$, $\eta_c \rightarrow K_S^0 K^\pm \pi^\mp$, a four-constraints (4C) kinematic fit is performed. The $\chi_{\text{5C}}^2 < 25$ and $\chi_{\text{4C}}^2 < 40$ are further required for the decay mode $\eta_c \rightarrow K^+ K^- \pi^0$ and $\eta_c \rightarrow K_S^0 K^\pm \pi^\mp$, respectively. These values are determined by optimizing the Figure-of-Merit (FOM) $S/\sqrt{S+B}$, where S represents the number of signal events from MC simulation, and B represents the number of normalized background events estimated from the left-hand sideband region of η_c in the data.

For each event, if there are multiple combinations satisfying the above criteria, only the combination with the minimum $\chi_{\text{tot}}^2 = \chi_{\text{4C}}^2 + \chi_{\text{1C}}^2 + \chi_{\text{PID}}^2 + \chi_{\text{vertex}}^2$ is kept, where χ_{4C}^2 is from the 4C kinematic fit for four-momentum conservation, χ_{1C}^2 is from the 1C kinematic fit for π^0 mass (this term is considered only in $\eta_c \rightarrow K^+ K^- \pi^0$ mode), χ_{PID}^2 is the sum of the $\chi_{\text{PID}}^2(i)$ for each charged track in the event, and χ_{vertex}^2 is from the K_S^0 secondary-

vertex fit (this term is only taken into account in the $\eta_c \rightarrow K_S^0 K^\pm \pi^\mp$ mode).

The background events from $\psi(2S) \rightarrow \pi^+ \pi^- J/\psi$ process in both channels are suppressed by requiring the recoil mass of $\pi^+ \pi^-$ to be less than $3.07 \text{ GeV}/c^2$. The background events from the $\psi(2S) \rightarrow \omega K^+ K^-$ in the $\eta_c(2S) \rightarrow \pi^+ \pi^- \eta_c$, $\eta_c \rightarrow K^+ K^- \pi^0$ decay is excluded by requiring $|M_{\pi^0 \pi^+ \pi^-} - m_\omega| > 0.02 \text{ GeV}/c^2$, where $M_{\pi^0 \pi^+ \pi^-}$ is the invariant mass of $\pi^0 \pi^+ \pi^-$ and m_ω is the known mass of ω [14].

B. Background estimation

A detailed study of the inclusive MC sample indicates that the backgrounds for $\eta_c(2S) \rightarrow \pi^+ \pi^- \eta_c$, $\eta_c \rightarrow K_S^0 K^\pm \pi^\mp$ process mainly come from (I) $\psi(2S) \rightarrow (\gamma_{\text{FSR}}) \pi^+ \pi^- K_S^0 K^\pm \pi^\mp$, where γ_{FSR} stands for a photon from final state radiation (FSR), (II) $\psi(2S) \rightarrow \gamma \eta_c(2S)$, $\eta_c(2S) \rightarrow \pi^+ \pi^- K_S^0 K^\pm \pi^\mp$, and (III) $\psi(2S) \rightarrow \gamma \chi_{c2}, \chi_{c2} \rightarrow \pi^+ \pi^- K_S^0 K^\pm \pi^\mp$. The background events in the $\eta_c(2S) \rightarrow \pi^+ \pi^- \eta_c$, $\eta_c \rightarrow K^+ K^- \pi^0$ process mainly come from (I) $\psi(2S) \rightarrow (\gamma_{\text{FSR}}) \pi^+ \pi^- K^+ K^- \pi^0$; (II) $\psi(2S) \rightarrow \pi^0 \pi^+ \pi^- \eta_c$, $\eta_c \rightarrow K^+ K^- \pi^0$; (III) $\psi(2S) \rightarrow \gamma \eta_c(2S)$, $\eta_c(2S) \rightarrow \pi^+ \pi^- K^+ K^- \pi^0$, and (IV) $\psi(2S) \rightarrow \gamma \chi_{c2}, \chi_{c2} \rightarrow \pi^+ \pi^- K^+ K^- \pi^0$. According to the studies of continuum data and inclusive MC sample, the contributions from continuum processes and events with misidentified π or K are found to be negligible. The remaining background channels with the same final states as the signal make only a small contribution, and the corresponding lineshapes are smooth within the $\pi^+ \pi^- K^+ K^- \pi^0$ or $\pi^+ \pi^- K_S^0 K \pi$ invariant mass spectrum, which are described by the MC shape generated uniformly in PHSP.

The backgrounds from $\psi(2S) \rightarrow \pi^+ \pi^- K_S^0 K^\pm \pi^\mp$ and $\psi(2S) \rightarrow \pi^+ \pi^- K^+ K^- \pi^0$, either with a fake photon or a real soft photon from FSR, produce a peak near the $\eta_c(2S)$ signal on the invariant mass spectrum of $\pi^+ \pi^- K_S^0 K^\pm \pi^\mp$ ($\pi^+ \pi^- K^+ K^- \pi^0$). This peak is shifted to a higher mass region after applying the three-constraints kinematic fit (3C) in which the energy of the M1 photon (M1 represents the magnetic dipole transition, the leading order transition amplitude. [34]) candidate is allowed to freely float [8]. The 3C fit keeps a similar mass resolution as the 4C fit and has better signal-background separation, as shown in Fig. 1, therefore, the result from the 3C fit is taken as the final mass spectrum. The contribution of such background is connected to the ratio f_{FSR} , which is defined as

$$f_{\text{FSR}} = \frac{N_{\text{FSR}}}{N_{\text{nonFSR}}}, \quad (1)$$

where N_{FSR} and N_{nonFSR} refer to the number of FSR events and non-FSR events, respectively. The relative ratio f_{FSR} between data and MC simulation is estimated to be 1.62 ± 0.13 using the control sample $\psi(2S) \rightarrow \gamma \chi_{c0}, \chi_{c0} \rightarrow 3(\pi^+ \pi^-)(\gamma_{\text{FSR}})$ [35].

The contributions of peaking backgrounds from

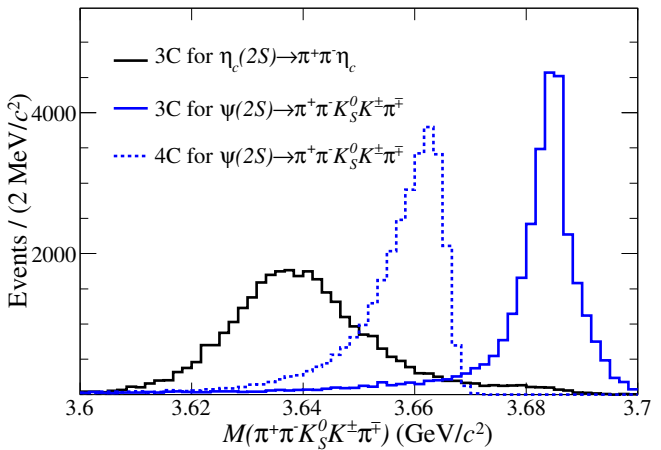


FIG. 1. Distributions of the invariant mass spectra of $\pi^+\pi^-K_S^0K^\pm\pi^\mp$ for $\eta_c(2S)\rightarrow\pi^+\pi^-\eta_c$, $\eta_c\rightarrow K_S^0K^\pm\pi^\mp$ process with 3C (black solid line), $\psi(2S)\rightarrow\pi^+\pi^-K_S^0K^\pm\pi^\mp$ process with 3C (blue solid line) and 4C kinematic fit (blue dashed line).

$\psi(2S)\rightarrow\gamma\eta_c(2S)$, $\eta_c(2S)\rightarrow\pi^+\pi^-K_S^0K^\pm\pi^\mp$ and $\eta_c(2S)\rightarrow\pi^+\pi^-K^+K^-\pi^0$ processes are determined by

$$N_{\text{bkg}}^{\text{peak}} = N_{\psi(2S)} \times \mathcal{B}_1 \times \mathcal{B}_2 \times \varepsilon, \quad (2)$$

where $N_{\psi(2S)}$ represents the total number of $\psi(2S)$ events, $\varepsilon = 4.9 \times 10^{-3}$ (2.0×10^{-3}) is the detection efficiency for $\eta_c(2S)\rightarrow\pi^+\pi^-K_S^0K^\pm\pi^\mp$ ($\pi^+\pi^-K^+K^-\pi^0$) mode. \mathcal{B}_1 is the branching fraction of $\psi(2S)\rightarrow\gamma\eta_c(2S)$ taken from the PDG [14]. \mathcal{B}_2 is the branching fraction of $\eta_c(2S)\rightarrow\pi^+\pi^-K_S^0K^\pm\pi^\mp$ ($\pi^+\pi^-K^+K^-\pi^0$), which is estimated to be $(1.33 \pm 1.04) \times 10^{-2}$, as discussed in Sec. IV ((1.4 ± 1.0) $\times 10^{-2}$ cited from the PDG [14]). With these inputs, the numbers of peaking background events $N_{\text{bkg}}^{\text{peak}}$ are determined to be 122 ± 36 and 54 ± 39 for $\eta_c(2S)\rightarrow\pi^+\pi^-K_S^0K^\pm\pi^\mp$ and $\eta_c(2S)\rightarrow\pi^+\pi^-K^+K^-\pi^0$ mode, respectively.

The background of $\psi(2S)\rightarrow\pi^+\pi^-K^+K^-\pi^0$ contributes a smooth component in the invariant mass spectrum of $\pi^+\pi^-K^+K^-\pi^0$ that is described by the MC-simulated shape.

C. Signal yield

We simultaneously fit the $\pi^+\pi^-K_S^0K^\pm\pi^\mp$ and $\pi^+\pi^-K^+K^-\pi^0$ invariant mass distributions with an unbinned maximum likelihood method to determine the number of signal events of $\eta_c(2S)\rightarrow\pi^+\pi^-\eta_c$.

The lineshape of $\eta_c(2S)$ produced by the M1 transition can be effectively described as

$$(E_\gamma^3 \times BW(m) \times f_d(E_\gamma)) \bigotimes F_{\text{res}} \times \varepsilon(m), \quad (3)$$

where m is the invariant mass of $\pi^+\pi^-K_S^0K^\pm\pi^\mp$

$(\pi^+\pi^-K^+K^-\pi^0)$, $E_\gamma = \frac{m_{\psi(2S)}^2 - m^2}{2m_{\psi(2S)}}$ is the energy of the transition photon in the rest frame of $\psi(2S)$, $BW(m)$ is the Breit-Wigner function for $\eta_c(2S)$. The mass and width of $\eta_c(2S)$ are fixed to 3643.4 MeV/ c^2 and 19.80 MeV, respectively, which are taken from the previous BESIII measurement [35]. $f_d(E_\gamma)$ is the function to damp the divergent tail raised by E_γ^3 [36],

$$f_d(E_\gamma) = \frac{E_0^2}{E_\gamma E_0 + (E_\gamma - E_0)^2}, \quad (4)$$

where $E_0 = \frac{m_{\psi(2S)}^2 - m_{\eta_c(2S)}^2}{2m_{\psi(2S)}}$. $\varepsilon(m)$ is the mass dependent efficiency function which is estimated by MC simulation. F_{res} is a double Gaussian function describing the detector resolution.

Events from $\psi(2S)\rightarrow\gamma\chi_{c2}, \chi_{c2}\rightarrow\pi^+\pi^-K_S^0K^\pm\pi^\mp/\pi^+\pi^-K^+K^-\pi^0$ are included in the fit. The lineshape of χ_{c2} is described by an MC shape convolved with a Gaussian function. The Gaussian function accounts for the difference in mass resolution between data and MC simulation, and its parameters are floated in the fit. The shape of the FSR processes, $\psi(2S)\rightarrow\gamma_{\text{FSR}}\pi^+\pi^-K^+K^-\pi^0$ and $\psi(2S)\rightarrow\gamma_{\text{FSR}}\pi^+\pi^-K_S^0K^\pm\pi^\mp$, as well as the $\psi(2S)\rightarrow\gamma\chi_{c2}$ and $\psi(2S)\rightarrow\pi^0\pi^+\pi^-K^+K^-\pi^0$ processes are fixed, while these background yields are floated in the fit. The yield of peaking background $\eta_c(2S)\rightarrow\pi^+\pi^-K_S^0K^\pm\pi^\mp$ ($\pi^+\pi^-K^+K^-\pi^0$) is fixed in the fit according to estimation in Sec. III B. The remaining backgrounds are described by a third-order Chebychev polynomial function with both the parameters and number of events are floated.

No significant $\eta_c(2S)$ signal is observed in the $\pi^+\pi^-K^+K^-\pi^0(\pi^+\pi^-K_S^0K^\pm\pi^\mp)$ invariant mass spectra after 3C kinematic fit. The fit results are displayed in Fig. 2. The fit qualities are $\chi^2/ndf_{\pi^+\pi^-K^+K^-\pi^0} = 1.59$ and $\chi^2/ndf_{\pi^+\pi^-K_S^0K^\pm\pi^\mp} = 1.26$, where ndf stands for the number of degrees of freedom.

D. Upper limit on branching fraction

The product branching fraction of $\mathcal{B}(\psi(2S)\rightarrow\gamma\eta_c(2S)) \times \mathcal{B}(\eta_c(2S)\rightarrow\pi^+\pi^-\eta_c)$ is calculated as

$$\mathcal{B} = \frac{N_{\text{sig}}}{N_{\psi(2S)} \times (\varepsilon_3 \times \mathcal{B}_3 + \varepsilon_4 \times \mathcal{B}_4)}. \quad (5)$$

Here, N_{sig} is the upper limit on the signal yield, \mathcal{B}_3 (\mathcal{B}_4) represents the branching fraction of η_c hadronic decay $\eta_c\rightarrow K^+K^-\pi^0$ ($\eta_c\rightarrow K_S^0K^\pm\pi^\mp$), and ε_3 (ε_4) is the efficiency obtained with MC simulation, which is 11.4% (12.0%) for $K^+K^-\pi^0$ ($K_S^0K^\pm\pi^\mp$) mode. An upper limit at the 90% C.L. for $\mathcal{B}(\psi(2S)\rightarrow\gamma\eta_c(2S)) \times \mathcal{B}(\eta_c(2S)\rightarrow\pi^+\pi^-\eta_c)$ is set using the Bayesian method [37]. The systematic uncertainties detailed in Section V are taken into account in the upper limit calculation. First, we select

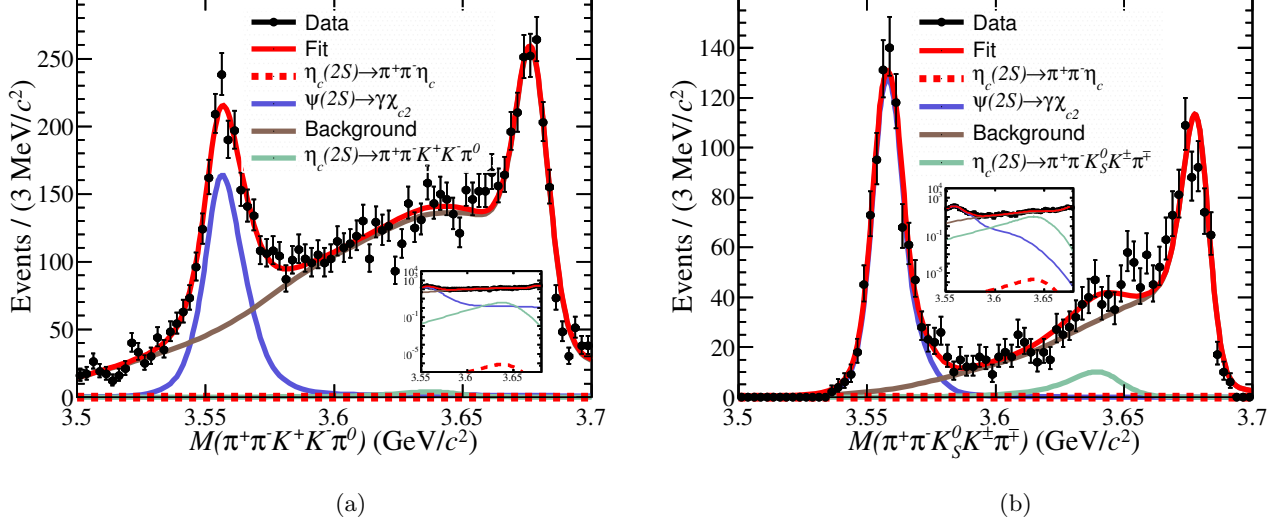


FIG. 2. The results of the simultaneous fit to the invariant mass distributions of (a) $M_{\pi^+\pi^-K^+K^-\pi^0}^{3C}$ and (b) $M_{\pi^+\pi^-K_S^0K_S^\pm\pi^\mp}^{3C}$, and the magnified view of the signal region on a logarithmic scale. The black dots with error bars are data, the blue solid lines are for $\psi(2S) \rightarrow \gamma\chi_{c2}$, the red dashed lines are the MC signals, the green solid lines are the peaking background components, the red solid lines are the total fit curves, and the brown solid lines represent the remaining backgrounds.

the likelihood that produces the largest upper limit with considering the additive systematic terms. To incorporate the multiplicative terms into branching fraction limit, the probability of the measured branching fraction $P(\mathcal{B})$ being determined using a maximum likelihood fit, is convolved with a probability density function of sensitivity, which is defined as the denominator of Eq. 5. The probability density function of sensitivity is assumed to be a Gaussian function with central value \hat{S} and standard deviation σ_s [38], which is given by

$$P'(\mathcal{B}) = \int_0^\infty P\left(\frac{S}{\hat{S}}\mathcal{B}\right) \exp\left[\frac{-(S - \hat{S})^2}{2\sigma_s^2}\right] dS, \quad (6)$$

where S and \hat{S} refer to the sensitivity, S is the variable of integration and σ_s is its multiplicative systematics which is discussed in Section V. By scanning $P'(\mathcal{B})$, the branching fraction upper limit at the 90% C.L. is calculated to be 2.21×10^{-5} via the following equation

$$0.9 = \int_0^{\mathcal{B}^{up}} P'(\mathcal{B}) d\mathcal{B}. \quad (7)$$

The normalized likelihood distribution as a function of $\mathcal{B}(\psi(2S) \rightarrow \gamma\eta_c(2S)) \times \mathcal{B}(\eta_c(2S) \rightarrow \pi^+\pi^-\eta_c)$, taking into account the systematic uncertainties is shown in Fig. 3.

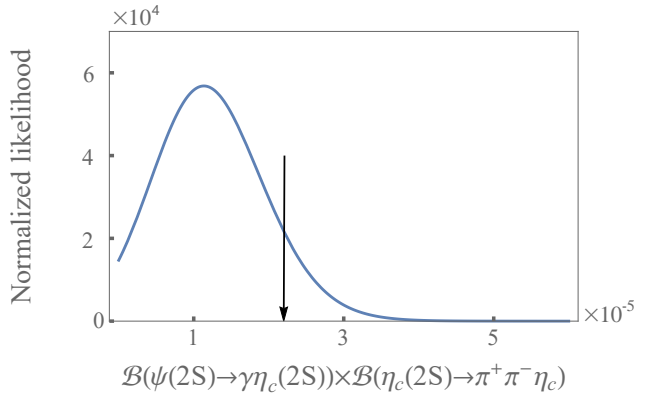


FIG. 3. Normalized likelihood versus the $\mathcal{B}(\psi(2S) \rightarrow \gamma\eta_c(2S)) \times \mathcal{B}(\eta_c(2S) \rightarrow \pi^+\pi^-\eta_c)$ after taking into account the systematic uncertainties. The black arrow corresponds to the product branching fraction at the 90% C.L. upper limit.

IV. MEASUREMENT OF $\eta_c(2S) \rightarrow \pi^+\pi^-K_S^0K_S^\pm\pi^\mp$

A. Event selection

The selection criteria for $\eta_c(2S) \rightarrow \pi^+\pi^-K_S^0K_S^\pm\pi^\mp$ decay are almost the same as those for $\psi(2S) \rightarrow \gamma\eta_c(2S)$, $\eta_c(2S) \rightarrow \pi^+\pi^-\eta_c$, $\eta_c \rightarrow K_S^0K_S^\pm\pi^\mp$, as described in Section III A. But, the selection criteria for

¹⁰⁶ η_c is removed. A 4C kinematic fit is performed under
¹⁰⁷ the $e^+e^- \rightarrow \gamma\pi^+\pi^-\pi^+\pi^-K_S^0K^\pm\pi^\mp$ hypothesis, and χ_{4C}^2 is
¹⁰⁸ further required to be less than 25.

¹⁰⁹ B. Background estimation

¹¹⁰ The analysis of the inclusive MC sample shows
¹¹¹ that the backgrounds mainly come from (I) $\psi(2S) \rightarrow$
¹¹² $(\gamma_{FSR})\pi^+\pi^-K_S^0K^\pm\pi^\mp$, (II) $\psi(2S) \rightarrow \pi^0\pi^+\pi^-K_S^0K^\pm\pi^\mp$,
¹¹³ (III) $\psi(2S) \rightarrow \gamma\chi_{c1,2}, \chi_{c1,2} \rightarrow \pi^+\pi^-K_S^0K^\pm\pi^\mp$, (IV)
¹¹⁴ continuum process, and (V) events with pion or kaon
¹¹⁵ misidentified.

¹¹⁶ The lineshapes for the invariant mass of $\pi^+\pi^-K_S^0K^\pm\pi^\mp$
¹¹⁷ are described with the corresponding MC shapes for
¹¹⁸ background process of (I) and (II). The lineshape of
¹¹⁹ $\chi_{c1,2}$ is described with the MC shape convoluted with
¹²⁰ a Gaussian function for the difference in resolution of
¹²¹ $M(\pi^+\pi^-K_S^0K^\pm\pi^\mp)$ between data and MC simulation
¹²² for the process of (III), while the number of events of
¹²³ each component and parameters in the Gaussian function
¹²⁴ are floated in the final fit. The data sample collect-
¹²⁵ ed at $\sqrt{s} = 3.65$ GeV is used to estimate the background
¹²⁶ from the continuum process $e^+e^- \rightarrow \gamma\pi^+\pi^-K_S^0K^\pm\pi^\mp$.
¹²⁷ The momenta and energies of final state particles are
¹²⁸ scaled to account for the difference in center-of-mass en-
¹²⁹ ergy. The events passed the signal selection criteria are
¹³⁰ then normalized according to differences in integrated lu-
¹³¹ minosity and cross section. The normalization factor is
¹³² determined to be 9.8. To reduce the influence of statis-
¹³³ tical fluctuations, we model the shape of the background
¹³⁴ from the continuum process by the ARGUS function to-
¹³⁵ gether with a Gaussian function, as shown in Fig. 4, and
¹³⁶ the number of events considering the normalization fac-
¹³⁷ tor is fixed in the final fit. We describe all other back-
¹³⁸ grounds with the shapes fixed to those from the inclusive
¹³⁹ MC sample, while the number of events is floated in the
¹⁴⁰ final fit.
¹⁴¹

¹⁴² C. Signal yield

¹⁴³ The 4C kinematic fit is utilized in event selection, while
¹⁴⁴ the $M_{\pi^+\pi^-K_S^0K\pi}^{3C}$ distribution of the 3C kinematic fit is
¹⁴⁵ used for the signal measurement due to its improved
¹⁴⁶ signal-background separation. An unbinned maximum
¹⁴⁷ likelihood fit is performed. The lineshape of $\eta_c(2S)$ is
¹⁴⁸ described by Eq. 3.
¹⁴⁹

¹⁵⁰ Figure 5(a) displays all the different components in-
¹⁵¹ volved in the fit process, along with the relative pull dis-
¹⁵² tribution. The zoomed distribution of the fit result and
¹⁵³ the background-subtracted distribution in the $\eta_c(2S)$ sig-
¹⁵⁴ nificant region are depicted in Fig. 5(b). The yield of $\eta_c(2S)$,
¹⁵⁵ N'_{sig} , is determined to be 3140 ± 241 , with a statistical
¹⁵⁶ significance of 10σ calculated from the difference of the
¹⁵⁷ logarithmic likelihoods ($-2(\mathcal{L}_{sig} - \mathcal{L}_{bkg})$) taking into ac-
¹⁵⁸ count the difference in the ndf [39]. Here, \mathcal{L}_{sig} and \mathcal{L}_{bkg}
¹⁵⁹

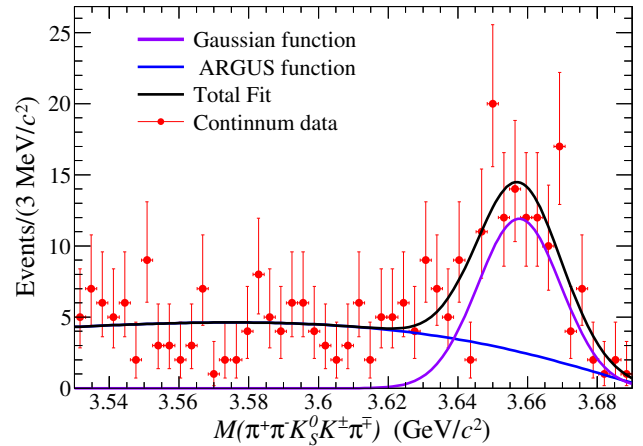


FIG. 4. Distribution of $M_{\pi^+\pi^-K_S^0K^\pm\pi^\mp}^{3C}$. The purple line is the Gaussian function, the blue line is the ARGUS function, the red dots with error bars are continuum data and the black line is the total fit curve.

are the negative logarithmic maximized likelihoods with and without a signal component, respectively.

D. Branching fraction

The product branching fraction $\mathcal{B}(\psi(2S) \rightarrow \gamma\eta_c(2S)) \times \mathcal{B}(\eta_c(2S) \rightarrow \pi^+\pi^-K_S^0K^\pm\pi^\mp)$ is calculated as

$$\mathcal{B}_{pro} = \frac{N'_{sig}}{N_{\psi(2S)} \times \varepsilon'}, \quad (8)$$

where $\varepsilon' = 12.4\%$ is the detection efficiency estimated by MC simulation. The branching fraction of $\eta_c(2S) \rightarrow \pi^+\pi^-K_S^0K^\pm\pi^\mp$ is determined to be $(1.33 \pm 0.11) \times 10^{-2}$, where the uncertainty is statistical only.

V. SYSTEMATIC UNCERTAINTY

A. Systematic uncertainty for $\eta_c(2S) \rightarrow \pi^+\pi^-\eta_c$

The sources of systematic uncertainties are divided into two categories: additive and multiplicative terms.

The additive uncertainties arise from the fit range, signal shape and background estimation. A conservative approach is adopted by considering all possible variations and selecting the one that yields the largest upper limit.

- (i) The systematic uncertainty arising from the fit range is determined by changing the invariant mass fit range from $[3.5, 3.7] \text{ GeV}/c^2$ to $[3.52, 3.72] \text{ GeV}/c^2$ and $[3.51, 3.71] \text{ GeV}/c^2$.
- (ii) The uncertainty associated with the η_c shape is estimated by changing damping function from

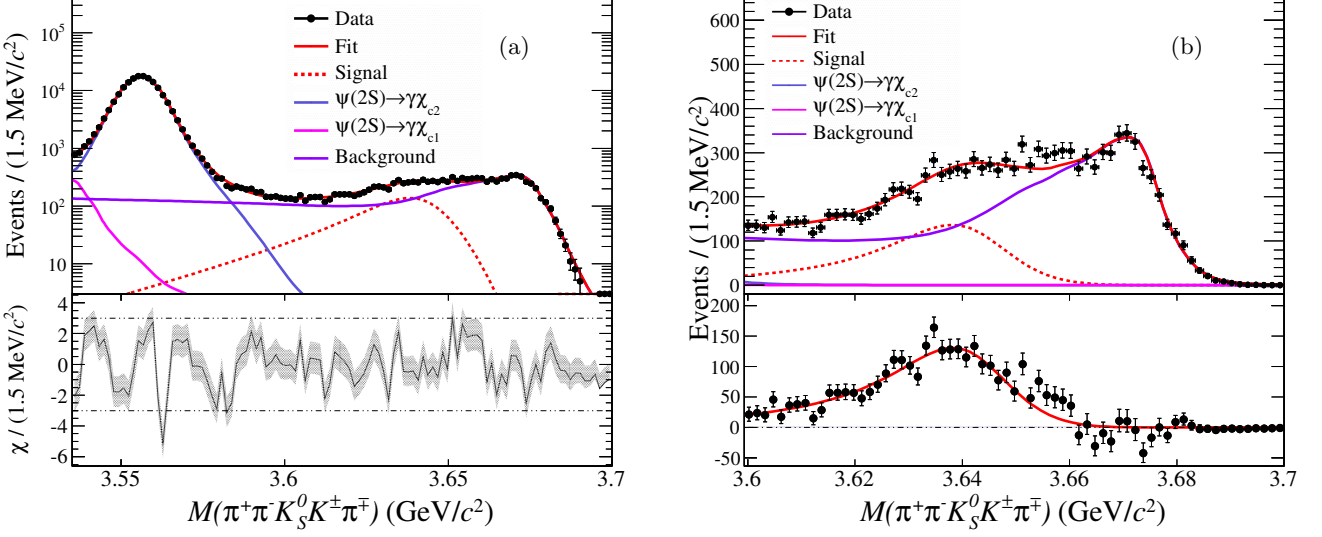


FIG. 5. (a) Distribution of $M_{\pi^+\pi^-K_S^0 K\pi}^{3C}$, the related fit result and the pull distribution. (b) Zoomed $M_{\pi^+\pi^-K_S^0 K\pi}^{3C}$ spectrum and background residuals. The black dots with error bars are data, the blue solid line is the lineshape of $\psi(2S) \rightarrow \gamma\chi_{c2}$, the pink solid line is the lineshape of $\psi(2S) \rightarrow \gamma\chi_{c1}$, the purple solid line is for the remaining background, the red dotted line is the signal, and the red solid line is the total fit result.

Eq. 4 to an alternative one used by the CLEO²¹⁰ Collaboration [40], while the mass parameter of the²¹¹ $\eta_c(2S)$ is varied by $\pm 1\sigma$. The systematic uncer-²¹² tainty caused by the resolution difference between²¹³ data and MC simulation in the decay $\eta_c(2S) \rightarrow$ ²¹⁴ $\pi^+\pi^-\eta_c$ is estimated by using the control samples²¹⁵ $\chi_{c2} \rightarrow \pi^+\pi^-K^+K^-\pi^0$ and $\chi_{c2} \rightarrow \pi^+\pi^-K_S^0 K^\pm\pi^\mp$.²¹⁶ The obtained mass resolution instead of the nomi-²¹⁷ nal one is used in the Gaussian function to describe²¹⁸ the $\eta_c(2S)$ shape.²¹⁹

(iii) The uncertainty due to the background shape is²¹⁹ estimated by altering the function from the third-²²⁰ order to the second-order Chebyshev polynomial²²¹ function. The relative ratio f_{FSR} is changed by²²² $\pm 1\sigma$ to evaluate the systematic uncertainty due to²²³ FSR. The uncertainty due to peaking background²²⁴ is estimated by varying the number of $\eta_c(2S) \rightarrow$ ²²⁵ $\pi^+\pi^-K_S^0 K^\pm\pi^\mp$ and $\eta_c(2S) \rightarrow \pi^+\pi^-K^+K^-\pi^0$ ²²⁶ events by $\pm 1\sigma$ for $\eta_c \rightarrow K_S^0 K^\pm\pi^\mp$ and $\eta_c \rightarrow$ ²²⁷ $K^+K^-\pi^0$ decay mode, respectively.²²⁸

The multiplicative uncertainties are involved in the de-²²⁹ termination of efficiency and branching fraction. These²³⁰ uncertainties include the following sources.²³¹

- (i) The uncertainty of the total number of $\psi(2S)$ events is estimated to be 0.5% [41].
- (ii) The uncertainty due to tracking efficiency for charged track is determined to be 1.0% per track using the control samples $J/\psi \rightarrow \pi^0\pi^+\pi^-$, $J/\psi \rightarrow p\bar{p}\pi^+\pi^-$ and $J/\psi \rightarrow K_S^0 K^\pm\pi^\mp + c.c.$ [42].

- (iii) The systematic uncertainty due to photon detection efficiency is 1.0% per photon, which is determined from the control samples $J/\psi \rightarrow \rho^0\pi^0$ and $e^+e^- \rightarrow \gamma\gamma$ [43].
- (iv) The systematic uncertainty due to K_S^0 reconstruction is studied using control samples $J/\psi \rightarrow K^{\pm}K^{\mp}$ and $J/\psi \rightarrow \phi K_S^0 K^\pm\pi^\mp$, and estimated to be 1.0%.
- (v) Using a high purity control sample of $J/\psi \rightarrow \pi^0\bar{p}p$, the systematic uncertainty from the π^0 reconstruction is determined to be 1.0% [44].
- (vi) The systematic uncertainty associated with the kinematic fit is assigned as the difference between the detection efficiencies before and after the helix parameter corrections [45] in the MC simulation, which is 2.0% for $\eta_c(2S) \rightarrow \pi^+\pi^-\eta_c$, $\eta_c \rightarrow K_S^0 K^\pm\pi^\mp$, and 2.5% for $\eta_c(2S) \rightarrow \pi^+\pi^-\eta_c$, $\eta_c \rightarrow K^+K^-\pi^0$ mode.
- (vii) To evaluate the uncertainty due to the J/ψ veto, we vary the requirement on the recoil mass of $\pi^+\pi^-$ pair by ± 10 MeV/ c^2 . The maximum deviation in the measured result is taken as the systematic uncertainty.
- (viii) The systematic uncertainty arising from the η_c mass window is estimated by adjusting the mass window by ± 10 MeV/ c^2 . The maximum difference in the branching fraction with respect to the nominal value is taken as the systematic uncertainty.

- (ix) To evaluate the uncertainty due to the ω veto, we change the mass window of ω by $\pm 1 \text{ MeV}/c^2$. The maximum deviation in the measured result is taken as the systematic uncertainty.
- (x) The uncertainties from the branching fractions of $\psi(2S) \rightarrow \gamma\eta_c(2S)$, $\eta_c \rightarrow K^+K^-\pi^0$ and $\eta_c \rightarrow K_S^0K^\pm\pi^\mp$ are 71.4% [14], 13.6% and 11.2% [33] respectively.

Table I summarizes the multiplicative systematic uncertainties. The combined relative systematic uncertainty is calculated by [46]

$$\sigma_{\text{sum}}^i = \frac{\sqrt{(\omega_1 \delta_1^i)^2 + (\omega_2 \delta_2^i)^2 + 2\omega_1 \omega_2 \rho_{12}^i \delta_1^i \delta_2^i}}{\omega_1 + \omega_2}, \quad (9)$$

of the product branching fraction $\mathcal{B}(\psi(2S) \rightarrow \gamma\eta_c(2S)) \times \mathcal{B}(\eta_c(2S) \rightarrow \pi^+\pi^-\eta_c)$ is determined to be 2.21×10^{-5} at the 90% C.L.. The $\eta_c(2S) \rightarrow \pi^+\pi^-K_S^0K^\pm\pi^\mp$ decay is observed with a statistical significance of 10σ for the first time. The $\mathcal{B}(\eta_c(2S) \rightarrow \pi^+\pi^-K_S^0K^\pm\pi^\mp)$ is measured to be $(1.33 \pm 0.11 \pm 0.4 \pm 0.95) \times 10^{-2}$, where the first and second uncertainties are statistical and systematic, respectively, and the third uncertainty is from the quoted $\mathcal{B}(\psi(2S) \rightarrow \gamma\eta_c(2S))$ [14]. The product branching fraction $\mathcal{B}(\psi(2S) \rightarrow \gamma\eta_c(2S)) \times \mathcal{B}(\eta_c(2S) \rightarrow \pi^+\pi^-K_S^0K\pi)$ is determined to be $(9.31 \pm 0.72 \pm 2.77) \times 10^{-6}$, which is consistent with the previous measurement [17].

ACKNOWLEDGMENTS

The BESIII Collaboration thanks the staff of BEPCII and the IHEP computing center for their strong support. This work is supported in part by National Key R&D Program of China under Contracts Nos. 2023YFA1606704, 2020YFA0406300, 2020YFA0406400; National Natural Science Foundation of China (NSFC) under Contracts Nos. 11635010, 11735014, 11835012, 11935015, 11935016, 11935018, 11961141012, 12025502, 12035009, 12035013, 12061131003, 12192260, 12192261, 12192262, 12192263, 12192264, 12192265, 12221005, 12225509, 12235017; the Chinese Academy of Sciences (CAS) Large-Scale Scientific Facility Program; the CAS Center for Excellence in Particle Physics (CCEPP); Joint Large-Scale Scientific Facility Funds of the NSFC and CAS under Contract No. U1832207; CAS Key Research Program of Frontier Sciences under Contracts Nos. QYZDJ-SSW-SLH003, QYZDJ-SSW-SLH040; 100 Talents Program of CAS; The Institute of Nuclear and Particle Physics (INPAC) and Shanghai Key Laboratory for Particle Physics and Cosmology; European Union's Horizon 2020 research and innovation programme under Marie Skłodowska-Curie grant agreement under Contract No. 894790; German Research Foundation DFG under Contracts Nos. 455635585, Collaborative Research Center CRC 1044, FOR5327, GRK 2149; Istituto Nazionale di Fisica Nucleare, Italy; Ministry of Development of Turkey under Contract No. DPT2006K-120470; National Research Foundation of Korea under Contract No. NRF-2022R1A2C1092335; National Science and Technology fund of Mongolia; National Science Research and Innovation Fund (NSRF) via the Program Management Unit for Human Resources & Institutional Development, Research and Innovation of Thailand under Contract No. B16F640076; Polish National Science Centre under Contract No. 2019/35/O/ST2/02907; The Swedish Research Council; U. S. Department of Energy under Contract No. DE-FG02-05ER41374

B. Systematic uncertainties for $\eta_c(2S) \rightarrow \pi^+\pi^-K_S^0K\pi$

The systematic uncertainties in the measurement of the branching fraction of $\eta_c(2S) \rightarrow \pi^+\pi^-K_S^0K\pi$ are summarized in Table II.

The systematic uncertainty due to the tracking efficiency, photon reconstruction, K_S^0 reconstruction, total number of $\psi(2S)$ events, kinematic fit, J/ψ veto, fit range, and signal shape are estimated by the same method introduced in Sec. V A.

The systematic uncertainty due to the background is estimated by changing the relative ratio f_{FSR} and changing the parameterisation of continuum background.

VI. SUMMARY

Based on $(27.12 \pm 0.14) \times 10^8$ $\psi(2S)$ events collected by the BESIII detector, we search for the decays $\eta_c(2S) \rightarrow \pi^+\pi^-K_S^0K^\pm\pi^\mp$, and $\eta_c(2S) \rightarrow \pi^+\pi^-\eta_c$ with $\eta_c \rightarrow K_S^0K^\pm\pi^\mp$ and $\eta_c \rightarrow K^+K^-\pi^0$. No significant signal of $\eta_c(2S) \rightarrow \pi^+\pi^-\eta_c$ is observed, and the upper limit

TABLE I. Multiplicative systematic uncertainties (in %) in the measured branching fraction for $\eta_c(2S) \rightarrow \pi^+ \pi^- \eta_c$.

Source	$\eta_c(2S) \rightarrow \pi^+ \pi^- \eta_c, \eta_c \rightarrow K_S^0 K^\pm \pi^\mp$	$\eta_c(2S) \rightarrow \pi^+ \pi^- \eta_c, \eta_c \rightarrow K^+ K^- \pi^0$	σ_{sum}^i
$N_{\psi(2S)}$	0.5	0.5	0.5
Tracking efficiency	6.0	4.0	5.4
Photon reconstruction	1.0	3.0	1.6
K_S^0 reconstruction	1.0	-	0.7
π^0 reconstruction	-	1.0	0.3
Kinematic fit	2.0	2.5	2.1
J/ψ veto	4.4	4.0	3.3
η_c mass window	4.0	4.0	3.1
ω veto	-	0.1	0.03
η_c decay	11.2	13.6	8.9
Total	14.2	15.8	11.7
$\mathcal{B}(\psi(2S) \rightarrow \gamma \eta_c(2S))$	71.4		

TABLE II. Relative systematic uncertainties (%) in the measurement of the product branching fraction $\mathcal{B}(\psi(2S) \rightarrow \gamma\eta_c(2S)) \times \mathcal{B}(\eta_c(2S) \rightarrow \pi^+\pi^-K_S^0K\pi)$.

Source	Uncertainty
$N_{\psi(2S)}$	0.5
Tracking efficiency	6.0
Photon reconstruction	1.0
K_S^0 reconstruction	1.0
Kinematic fit	2.0
J/ψ veto	3.8
Fit range	3.8
Signal shape	18.9
Background estimation	21.5
Total	29.8

-
- 336 [1] N. Brambilla *et al.*, *J High Energy Phys.* **07**, 096 (2011),³⁷⁹
337 arXiv:1105.4807 [hep-ph].³⁸⁰
- 338 [2] S. K. Choi *et al.* (Belle Collaboration), *Phys. Rev. Lett.* **89**,³⁸¹
339 **102001** (2002), [Erratum: *Phys. Rev. Lett.* 89, 129901,³⁸²
340 (2002)], arXiv:hep-ex/0206002.³⁸³
- 341 [3] B. Aubert *et al.* (BaBar Collaboration), *Phys. Rev. Lett.* **92**,³⁸⁴
342 **142002** (2004), arXiv:hep-ex/0311038.³⁸⁵
- 343 [4] K. K. Seth (CLEO Collaboration), *AIP Conf. Proc.* **717**,³⁸⁶
344 **543** (2004).³⁸⁷
- 345 [5] H. Nakazawa *et al.* (Belle Collaboration), *Nucl. Phys. B*³⁸⁸
346 *Proc. Suppl.* **184**, 220 (2008).³⁸⁹
- 347 [6] B. Aubert *et al.* (BaBar Collaboration), *Phys. Rev. D* **72**,³⁹⁰
348 **031101** (2005), arXiv:hep-ex/0506062.³⁹¹
- 349 [7] K. Abe *et al.* (Belle Collaboration), *Phys. Rev. Lett.* **98**,³⁹²
350 **082001** (2007).³⁹³
- 351 [8] M. Ablikim *et al.* (BESIII Collaboration), *Phys. Rev. Lett.* **109**,³⁹⁴
352 **042003** (2012).³⁹⁵
- 353 [9] G. S. Abrams *et al.*, *Phys. Rev. Lett.* **34**, 1181 (1975).³⁹⁶
- 354 [10] M. B. Voloshin, *JETP Lett.* **21**, 347 (1975).³⁹⁷
- 355 [11] L. S. Brown *et al.*, *Phys. Rev. Lett.* **35**, 1 (1975).³⁹⁸
- 356 [12] M. B. Voloshin, *Mod. Phys. Lett. A* **17**, 1533 (2002),³⁹⁹
357 arXiv:hep-ph/0206240.⁴⁰⁰
- 358 [13] J. Z. Bai *et al.* (BES), *Phys. Rev. D* **62**, 032002 (2000),⁴⁰¹
359 arXiv:hep-ex/9909038.⁴⁰²
- 360 [14] R. L. Workman *et al.* (Particle Data Group), *PTEP* **2022**,⁴⁰³
361 **083C01** (2022).⁴⁰⁴
- 362 [15] M. B. Voloshin, *Phys. Rev. D* **74**, 054022 (2006),⁴⁰⁵
363 arXiv:hep-ph/0606258.⁴⁰⁶
- 364 [16] J. P. Lees *et al.* (BaBar Collaboration), *Phys. Rev. D* **86**,⁴⁰⁷
365 **092005** (2012), arXiv:1206.2008 [hep-ex].⁴⁰⁸
- 366 [17] M. Ablikim *et al.* (BESIII Collaboration), *Phys. Rev. D* **87**,⁴⁰⁹
367 **052005** (2013), arXiv:1301.1476 [hep-ex].⁴¹⁰
- 368 [18] M. Ablikim *et al.* (BESIII Collaboration), *Nucl. Instrum. Meth. A* **614**,⁴¹¹
369 345 (2010).⁴¹²
- 370 [19] F. A. Harris, *Int. J. Mod. Phys. A* **24**, 0904370 (2008).⁴¹³
- 371 [20] M. Ablikim *et al.* (BESIII), *Chin. Phys. C* **44**, 040001,⁴¹⁴
372 (2020), arXiv:1912.05983 [hep-ex].⁴¹⁵
- 373 [21] J.-W. Zhang *et al.*, *Radiat. Detect. Technol. Methods* **6**,⁴¹⁶
374 **289** (2022).⁴¹⁷
- 375 [22] X. Li *et al.*, *Radiat. Detect. Technol. Methods* **1**, 13418
376 (2017).
- 377 [23] Y.-X. Guo *et al.*, *Radiat. Detect. Technol. Methods* **1**, 15
378 (2017).
- [24] P. Cao *et al.*, *Nucl. Instrum. Meth. A* **953**, 163053 (2020).
- [25] S. Agostinelli *et al.* (GEANT4), *Nucl. Instrum. Meth. A* **506**, 250 (2003).
- [26] S. Jadach, B. F. L. Ward, and Z. Was, *Comput. Phys. Commun.* **130**, 260 (2000), arXiv:hep-ph/9912214.
- [27] S. Jadach, B. F. L. Ward, and Z. Was, *Phys. Rev. D* **63**,
113009 (2001), arXiv:hep-ph/0006359.
- [28] D. J. Lange, *Nucl. Instrum. Meth. A* **462**, 152 (2001).
- [29] R.-G. Ping, *Chin. Phys. C* **32**, 599 (2008).
- [30] J. C. Chen, G. S. Huang, X. R. Qi, D. H. Zhang, and Y. S. Zhu, *Phys. Rev. D* **62**, 034003 (2000).
- [31] R.-L. Yang, R.-G. Ping, and H. Chen, *Chin. Phys. Lett.* **31**, 061301 (2014).
- [32] W. M. Tanenbaum *et al.*, *Phys. Rev. D* **17**, 1731 (1978).
- [33] M. Ablikim *et al.* (BESIII Collaboration), *Phys. Rev. D* **86**, 092009 (2012), arXiv:1209.4963 [hep-ex].
- [34] E. Eichten, S. Godfrey, H. Mahlke, and J. L. Rosner, *Rev. Mod. Phys.* **80**, 1161 (2008), arXiv:hep-ph/0701208.
- [35] M. Ablikim *et al.* (BESIII Collaboration), *Phys. Rev. D* **106**, 032014 (2022), arXiv:2206.08807 [hep-ex].
- [36] V. V. Anashin *et al.*, *Chin. Phys. C* **34**, 831 (2010), arXiv:1002.2071 [hep-ex].
- [37] J. Conrad *et al.*, *Phys. Rev. D* **67**, 012002 (2003), arXiv:hep-ex/0202013.
- [38] K. Stenson, arXiv:physics/0605236 [physics.data-an].
- [39] S. S. Wilks, *Annals Math. Statist.* **9**, 60 (1938).
- [40] R. E. Mitchell (CLEO Collaboration), *Physical Review Letters* **102**, 011801 (2008).
- [41] M. Ablikim *et al.* (BESIII Collaboration), *Chin. Phys. C* **42**, 023001 (2018), arXiv:1709.03653 [hep-ex].
- [42] M. Ablikim *et al.* (BESIII Collaboration), *Phys. Rev. D* **83**, 112005 (2011), arXiv:1103.5564 [hep-ex].
- [43] M. Ablikim *et al.* (BESIII Collaboration), *Phys. Rev. D* **81**, 052005 (2010), arXiv:1001.5360 [hep-ex].
- [44] M. Ablikim *et al.* (BESIII Collaboration), *Phys. Rev. Lett.* **105**, 261801 (2010), arXiv:1011.0885 [hep-ex].
- [45] M. Ablikim *et al.* (BESIII Collaboration), *Phys. Rev. D* **87**, 012002 (2013), arXiv:1208.4805 [hep-ex].
- [46] M. Ablikim *et al.* (BESIII Collaboration), *Phys. Rev. D* **107**, 072003 (2023), arXiv:2210.06988 [hep-ex].